POST-TEST ANALYSES OF SODIUM–SULPHUR CELLS AND AQUEOUS BATTERIES*

J. E. BATTLES, J. A. SMAGA and J. J. MARR

Argonne National Laboratory, 9700 South Cass Avenue, Argonne, IL 60439 (U.S.A.)

Post-test examinations are conducted at Argonne National Laboratory to obtain quantitative information on electrode morphology, corrosion and degradation of the cell hardware, and mechanisms responsible for existing or future cell failures. These findings are reported to the organizations responsible for the construction of these cells and support their efforts in achieving improved cell performance, cycle life, and reliability. This paper presents results of post-test analyses of recent high-temperature sodium/sulfur cells, and of aqueous lead–acid and nickel/iron batteries. In particular, the relationship between electrode performance and electrode morphology is examined for each of the three battery systems.

The sodium/sulfur cells for examination were fabricated and tested by Ford Aerospace & Communication Corp. An inert-atmosphere metallographic facility is used to perform these examinations because of the reactive nature of sodium and sodium polysulfides (Na_2S_x) with oxygen and/or moisture. After a cell is sectioned in a separate glove box, the samples are transferred to this facility. The large glove box contains all the equipment needed for complete sample preparation (mounting, grinding, and polishing) and a communicating glove box that houses a metallograph for microscopic examination [1]. Samples for additional analyses, such as wet chemistry, X-ray diffraction, and scanning electron microscopy, are also prepared in this facility and are transported to the respective instruments in sealed containers.

The sulfur electrode morphology has been found to be highly dependent upon the state of charge at termination and the length of cell operation [2]. As would be expected, the phases present in the microstructure at ambient temperature reflect the overall composition of the positive electrode melt; however, the determination of concentration gradients is complicated by the formation of metastable phases in addition to the predicted equilibrium phases (sulfur, Na_2S_5, Na_2S_4, Na_2S_2). The formation of five re-occurring metastable polysulfide phases has been established and confirmed by X-ray diffraction.

*The submitted manuscript has been authored by a contractor of the U.S. Government under contract No. W-31-109-ENG-38. Accordingly, the U.S. Government retains a nonexclusive, royalty-free license to publish or reproduce the published form of this contribution, or allow others to do so, for U.S. Government purposes.

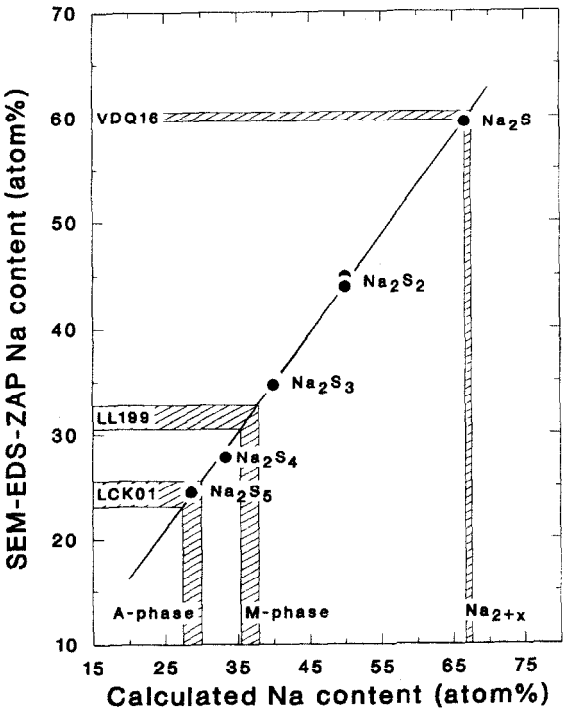

Fig. 1. The compositions of unknown Na_2S_x phases are determined with this curve. The SEM–EDS data (y-axis) underestimate the Na content because of its low atomic weight. Adjusted values (x-axis) are derived by using the calibration curve generated for standards (●) of known composition.

Scanning electron microscopy in conjunction with energy dispersive spectroscopy (SEM–EDS) is proving to be an effective method of deriving estimates for compositions of the metastable phases. In using the SEM–EDS technique, the spectra for the metastable phases are compared with polysulfide standards of known composition. These standards were prepared according to the procedure of Brown and Battles [3]. Figure 1 presents compositional data for two of the metastable phases. The gradients within the positive electrode can be mapped out with greater accuracy once the compositions of all the metastable phases are established.

The morphological studies indicate that severe concentration gradients do not develop until the two-liquids composition range is reached. Two reaction fronts are operative during this portion of a charging cycle range. A semicontinuous ring of sulfur develops around the polysulfide-coated electrolyte tube, and a second concentric sulfur ring forms near the container wall. The latter semicontinuous ring makes direct contact with portions of the container wall. Both rings tend to extend along the full length of the electrode, and small voids are often concentrated along the interface between the sulfur and the polysulfides. The polysulfides in these electrodes

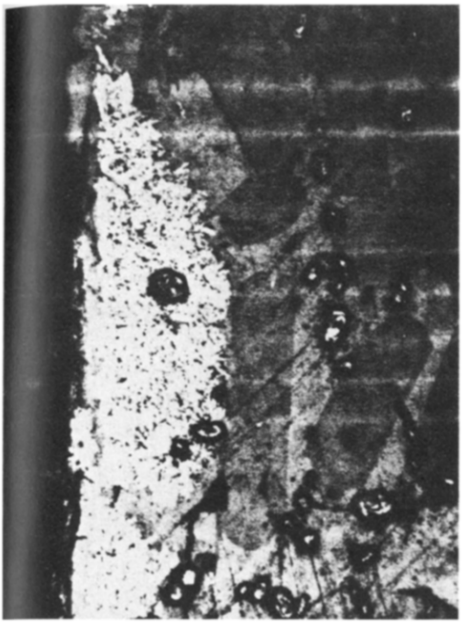

Fig. 2. Repeated cycles of scale formation, spallation, dissolution, and $NaCrS_2$ precipitation lead to the development of this 125 μm thick deposit (white) on the electrolyte surface.

include Na_2S_5 and the metastable S-, A-, and T-phases, with the latter two phases predominating. The SEM–EDS results for the A-phase (Fig. 1) and the X-ray diffraction data for the T-phase, which match a pattern reported by other investigators [4], indicate that both of these phases are metastable variants of Na_2S_5.

Examinations of cells of advanced cycle life indicate that the major cause of capacity decline is the deposition of corrosion products along the length of the electrolyte tube. Corrosion of the chromium-plated containers forms a scale that is rich in $NaCrS_2$. This scale reaches a limiting thickness and spalls away from the container. The $NaCrS_2$ dissolves in the melt and migrates to the electrolyte tube under the influence of potential or compositional gradients. Deposits, such as shown in Fig. 2, develop on or near the electrolyte surface when the localized concentration exceeds the solubility limit. The thickness of these deposits increases with cycle life. The detrimental influence of the $NaCrS_2$ buildup on the electrochemical performance of the cell is reflected in the electrode morphology away from the electrolyte. A "fully charged", life-tested cell will show sulfur rings that are comparable in development and thickness with the rings found in a cell terminated in the semicharged state after a few cycles.

These examinations also prove invaluable in identifying the origin of an electrolyte fracture, the major cause of cell failure. Primary fractures are differentiated from subsequent cracks by the presence of lower sodium polysulfides (Na_2S and Na_2S_2) in one or both electrodes adjacent to the fracture area.

Post-test examinations of two aqueous battery systems — lead–acid and nickel/iron — were conducted after the batteries had either failed or completed their testing at Argonne National Battery Testing Laboratory. Each battery was subjected to physical, chemical, and instrumental analyses to identify the cause of its performance degradation or failure.

Mechanical defects or physical changes of the active material resulting from the testing were determined by visual inspection of the exterior of the module and its disassembled components. Individual cell voltages and half-cell potentials were measured to determine the relative condition of the cells. Techniques such as radiography, optical and scanning electron microscopy, image analysis, X-ray diffraction, energy dispersive spectroscopy, X-ray image mapping, and wet chemistry analysis were used to provide quantitative measurements of grid corrosion, positive active materials softening and shedding, and changes in the negative electrode. These techniques were also used to determine the electrode morphology and to establish the distribution and composition of the electrode phases.

In the case of the lead–acid battery system, post-test examinations have identified the positive electrode as the usual offending component. Failure or capacity decline occurred because of active material degradation (in the form of coralloidal PbO_2 formation and eventual shedding) and positive grid corrosion. The coralloidal structure of PbO_2 observed in the positive active material appears to be a common behavior. A typical corroded positive grid is shown in Fig. 3. As seen in Fig. 3, an oxidized layer with cracks parallel to the paste/grid interface can be found. The resulting loss of contact due to the cracks between the grid and the active material might have increased the electrode resistance and reduced the battery capacity.

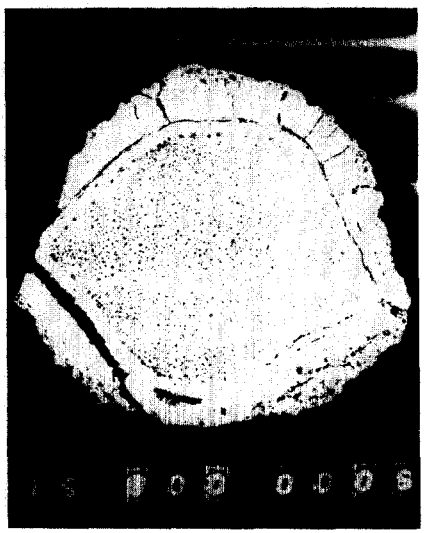

Fig. 3. A cross section of the positive grid of a lead–acid battery showing corrosion and spallation of the corrosion layer.

Iron contamination of the nickel electrode was found to be the primary failure mode of the nickel/iron batteries. X-ray image mapping of the nickel electrode cross section showed a high iron concentration in the outer layer of the nickel electrode (approx. 25 μm in thickness). X-ray diffraction analysis of this layer revealed that the iron was in the form of a nickel iron oxide compound (namely, ferroan trevorite). The formation of this compound might play a very important role in the capacity loss of the nickel/iron battery.

References

1 J. E. Battles, F. C. Mrazek and N. C. Otto, Post-test examination of Li–Al/FeS_x secondary cells, *ANL-80-130, December, 1980.* See also F. C. Mrazek, *Microscope, 31* (1983) 235.
2 J. A. Smaga, B. S. Tani, J. E. Battles and R. W. Minck, *Ext. Abstr., 166th Electrochem. Soc. Meeting, New Orleans, LA, October 7 - 12, 1984, 84-2* (1984) 160.
3 A. P. Brown and J. E. Battles, *Synth. React. Inorg. Met. Org. Chem., 14* (1984) 945.
4 G. J. Janz *et al.*, *Inorg. Chem., 15* (1976) 1759.